

Numerical Investigation of Vortex Structures in the Rim Cavities of Gas Turbines

Ulvi Fatullayev¹

¹Duisburg, Germany

Orcid Id: 0009-0000-0851-5509

Publication Date: 2025/06/11

Abstract: This study presents a computational investigation of vortex structures forming within the rim cavities of gas turbines. Utilizing computational fluid dynamics (CFD), both steady-state and transient simulations were conducted on simplified cavity models derived from a 1.5-stage experimental turbine. A range of cavity widths and boundary conditions, including surface-averaged and profile-based inlets and outlets, were explored. The emergence of large-scale rotating structures and Kelvin-Helmholtz instabilities was evaluated under varying non-dimensional purge flow rates at a low non-dimensional purge flow rate. Time-resolved simulations showed the importance of realistic profile boundary conditions in capturing the unsteady flow phenomena. The analysis confirmed the sensitivity of vortex formation to geometric and flow conditions, particularly the boundary specification and purge flow magnitude. Transient simulations using profile inlet velocity and outlet pressure distributions yielded results closely matching experimental observations. These findings contribute to optimizing secondary air systems and improving turbine cooling efficiency while reducing unnecessary purge air usage.

Keywords: Gas Turbines, Rim Cavity, CFD, Vortex Structures, Hot Gas Ingestion, Purge Flow, Kelvin-Helmholts Instabilities.

How to Cite: Ulvi Fatullayev. (2025). Numerical Investigation of Vortex Structures in the Rim Cavities of Gas Turbines. *International Journal of Innovative Science and Research Technology*, 10(6), 103-115. <https://doi.org/10.38124/ijisrt/25jun048>.

I. INTRODUCTION

Gas turbines are indispensable in various engineering applications, including power generation, aviation, and mechanical drives, due to their ability to convert thermal energy into mechanical work efficiently. Fundamentally, gas turbines consist of three primary components: the compressor, combustion chamber, and turbine. Air is drawn in by the compressor, compressed, and subsequently mixed with fuel and ignited in the combustion chamber. The resulting high-pressure, high-temperature gases expand through the turbine, producing work that is used both to drive the compressor and generate power or thrust.

A typical approach to increasing the efficiency of gas turbines is to elevate the turbine inlet temperature. However, this method is constrained by the thermal limits of the turbine materials. Therefore, innovative cooling strategies

must be adopted to prevent component degradation. Among these strategies, the secondary air system plays a vital role. It delivers cooling air to critical regions, including the rim cavities between rotating and stationary discs, where hot gas ingestion poses a significant threat to mechanical integrity.

Approximately 20–25% of the total mass flow from the compressor is diverted into the secondary air system for cooling and sealing purposes. The effectiveness of this system depends heavily on the optimal extraction point, as it must balance thermal efficiency with cooling needs. Cooling air drawn from earlier compressor stages, where the pressure is lower, is thermodynamically more efficient and preserves compressor performance. Figure 1.1 illustrates the secondary flow paths in a Rolls-Royce gas turbine, highlighting the complexity and significance of effective secondary air management.

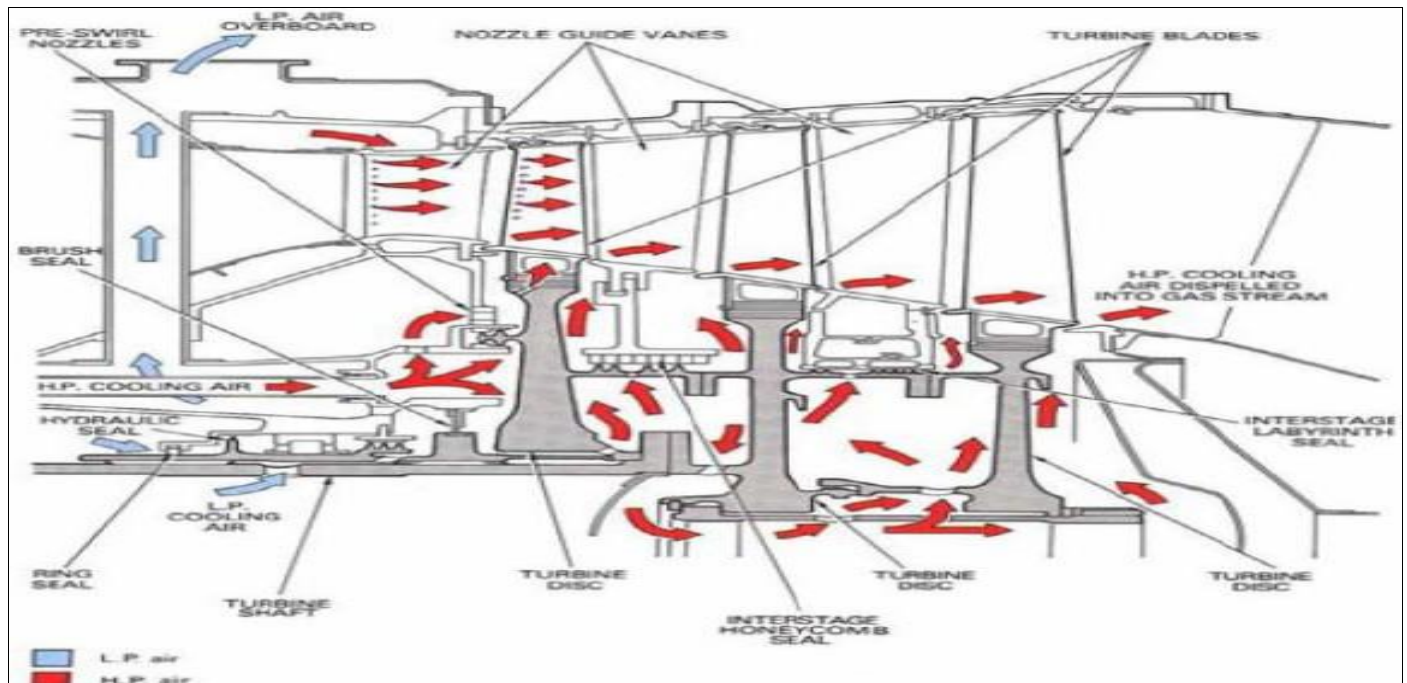


Fig 1.1: Secondary Flow Paths in a Rolls-Royce Gas Turbine[1]

Inadequate purge air can lead to the ingestion of hot gases into the wheel-space cavities, accelerating material degradation. Conversely, excessive purge flow reduces overall efficiency. Thus, accurately determining the required amount of purge air is critical to maintaining both performance and component lifespan. CFD has become an invaluable tool in addressing this challenge, enabling the simulation of flow behavior in these complex geometries.

Experimental studies, particularly those conducted at RWTH Aachen, have identified the formation of large-scale rotating structures within the turbine front cavities. These structures rotate at approximately 80% of the rotor speed and are most prominent at non-dimensional sealing flow rates (C_w) below 15,000. Complementary CFD simulations by C. Cao et al. [2] showed excellent agreement with these observations when using full 360° models.

Jacoby et al. [3], as part of the ICAS-GT2 European research program, emphasized the influence of circumferential pressure gradients and rotor pumping in promoting ingestion. Their research confirmed that realistic pressure disturbances must be included to capture the unsteady nature of cavity flows. The limitations of periodic boundary conditions were particularly evident in these studies, which often led to the suppression of flow disturbances incompatible with the domain's angular extent.

Julien et al. [4] further advanced these findings by investigating the effect of using larger periodic segments (up to 74°) in contrast to the 22.5° sectors used previously. Their results showed that larger sectors offered better prediction of vortex behavior due to improved representation of the pressure field.

Additionally, M. Rabs et al. [5] demonstrated that Kelvin-Helmholtz instabilities, resulting from the shear

between tangential hot gas and purge air, can develop within the rim seal cavity. These instabilities are influenced by cavity width and purge flow rate. Using the $k-\omega$ -SST turbulence model, their unsteady simulations captured the onset and evolution of these instabilities in both simplified and full-stage geometries.

Previous CFD analyses by Ellermann [6] explored vortex formation using swirl-free and profile-based boundary conditions. While his study demonstrated some unsteady behavior, the lack of realistic inflow profiles limited its predictive accuracy. Nevertheless, it provided a foundational understanding of the limitations of steady-state and simplified boundary condition modeling.

Hills et al. [7] and Chen et al. [8] earlier noted that CFD models often underpredict pressure gradients in the rim cavities when compared to experiments, particularly at low sealing flow rates. Their findings, along with King and Wilson [9], who examined buoyancy-driven vortices in rotating cavities, underscore the challenges of capturing the complex unsteady behavior of turbine internal flows.

In summary, both experimental and numerical investigations confirm that the development of large-scale rotating structures and Kelvin-Helmholtz instabilities depends on several interrelated factors, including the purge flow rate, cavity geometry, turbulence model, and boundary conditions. Despite the extensive body of research, CFD predictions still exhibit gaps under realistic configurations. The current study seeks to bridge this gap by conducting transient simulations under a low non-dimensional purge flow rate using refined inlet and outlet profile boundary conditions. The objective is to provide insights into the unsteady behavior of vortex structures and support the design of more efficient secondary air systems in gas turbines.

II. METHODOLOGY

A. Theoretical Background

The use of Computational Fluid Dynamics (CFD) to study unsteady flow behavior in turbine rim cavities has gained widespread adoption due to its ability to visualize internal flow fields with high spatial and temporal resolution. The complexity of rotating cavity flows, particularly in rim seals, involves interactions between secondary air systems, purge flows, and hot mainstream gases, which are challenging to capture without a robust numerical approach. Several studies have emphasized the necessity of modeling such systems with accurate turbulence closure and realistic boundary conditions to reproduce the observed phenomena such as vortex structures and ingestion mechanisms.

Turbulence modeling is fundamental in these simulations. The Shear Stress Transport (SST) model is particularly well-suited for this purpose as it blends the advantages of the $k-\epsilon$ and $k-\omega$ models. The SST model efficiently predicts near-wall behavior and flow separation regions, crucial for capturing instabilities such as Kelvin-Helmholtz structures and large-scale vortices in shear-dominated flows. Previous investigations, including the work by Rabs et al. [5], demonstrated that the SST model can capture flow instabilities within rim seal geometries without excessive computational cost.

Despite its strength, Reynolds-Averaged Navier-Stokes (RANS)-based modeling, including the SST model, has known limitations when dealing with fine-scale turbulence and transition effects. Large Eddy Simulation (LES) and

Direct Numerical Simulation (DNS) offer greater accuracy in resolving temporal fluctuations but are computationally intensive and impractical for parametric studies involving multiple geometries and boundary conditions, as noted by Chen et al. [8] and King and Wilson [9]. Thus, SST-RANS remains the most pragmatic choice for industrially relevant studies like the one undertaken here.

Boundary condition fidelity is another central aspect affecting simulation realism. Ellermann [6] found that using simplified surface-averaged inflow conditions, although computationally efficient, often leads to underprediction of unsteady phenomena. These conditions lack the circumferential pressure and velocity gradients required to initiate coherent vortex patterns. To address this, Jacoby et al. [3] and Julien et al. [4] introduced the concept of using profile-based boundary conditions derived from full-stage simulations. These profiles incorporate both axial and tangential components and better represent the real flow environment.

Furthermore, Chen et al. [8] and Hills et al. [7] emphasized that large-scale structures, such as the experimentally observed "Mercedes star" patterns, only materialize when pressure gradients and rotor-stator interactions are adequately modeled. Their findings support the idea that both time resolution and circumferential fidelity are required to observe ingestion-related instabilities and their evolution.

Figure 3.2 illustrates the schematic of hot gas ingestion at the rotor-stator interface, a key mechanism influencing rim seal cavity dynamics.

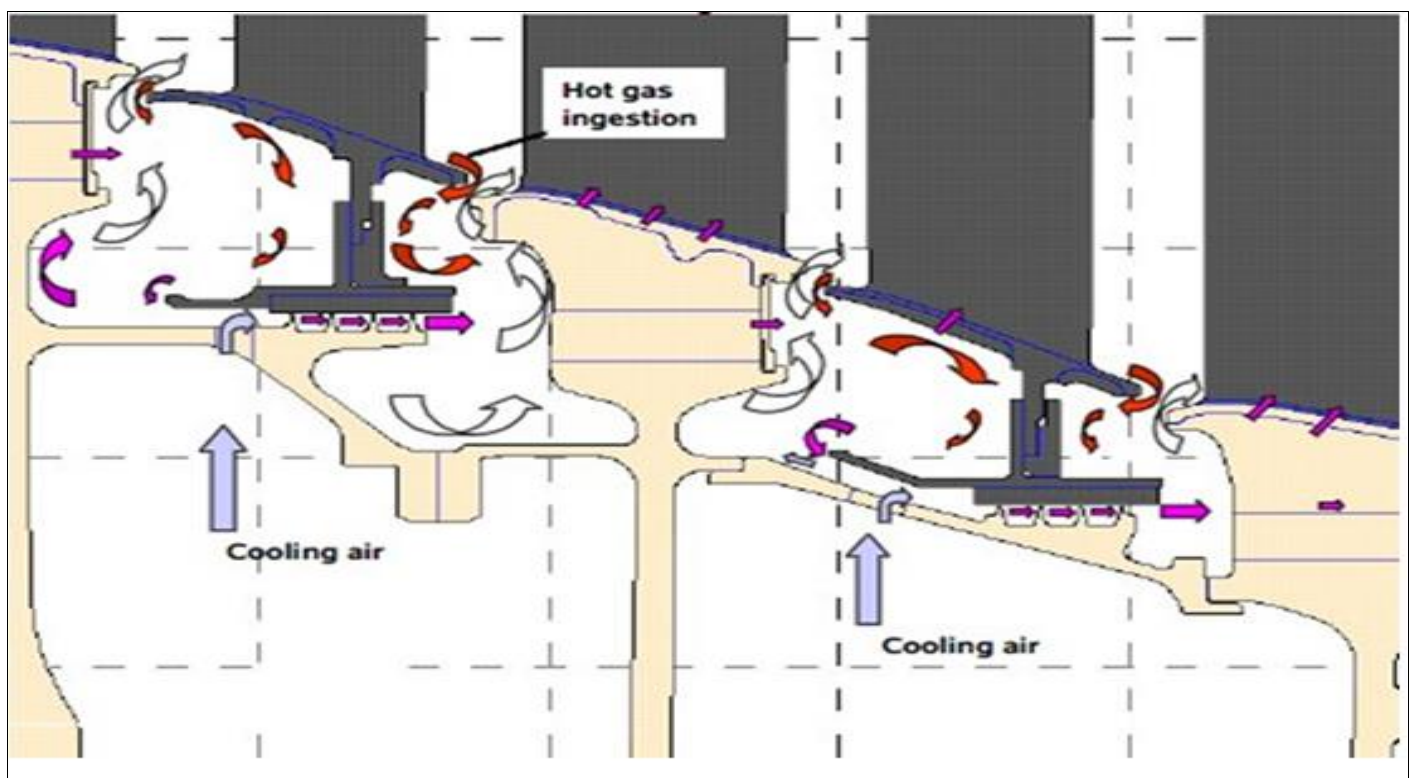


Fig 2.1: Schematic of Hot Gas Ingestion at the Rotor-Stator Interface

The time-dependent nature of vortex formation necessitates transient simulations with adequate time resolution. Time steps were selected to resolve flow features with sufficient fidelity while maintaining computational stability. Certain control parameters were also used to govern the stability, accuracy, and convergence behavior of the numerical method [10]. These included discretization schemes, convergence criteria, and under-relaxation factors, all of which influence solver robustness. Transforming velocity fields into a reference frame rotating at 80% of the rotor speed allowed for clearer identification of vortex structures and their trajectories, consistent with previous approaches by Cao et al. [2].

B. Model Description

All simulations have been performed using geometries based on a representative experimental setup, and all computational methods were selected with the aim of ensuring physically meaningful and computationally efficient outcomes. The description below outlines the modeling strategies used, the meshing specifications, and the approach to steady and transient simulations, while also clarifying the boundary conditions.

A periodic segment for the actual numerical simulations was extracted from the fluid flow path of the test rig in the Technical University of Aachen. The extracted

22.5° segment was later on transformed to its multiples (90°, 180°, 360°) in Ansys Preprocessor (CFX-Pre). The 22.5° was chosen, because it exactly matches the cavity between one vane and two blades in the test rig, which has a total of 16 vanes and 32 blades

In total, five different models were applied for the simulations in the framework of the actual investigations. All the models used are simplified cavity models without vanes and blades. These models are listed below:

- 90 degree segment standard model
- 180 degree segment standard model
- 360 degree standard model
- 90 degree model with cavity width 7.5 [mm]
- 90 degree model with cavity width 10.5 [mm]

The 90° segment models were particularly useful for studying the impact of cavity size on vortex development with reduced computational demand. These segment models are shown in Figure 4.2, which illustrates the baseline geometry and modifications introduced by varying the cavity width. The visualizations include (a) the baseline 3D model, (b) the 7.5 mm cavity configuration, (c) the 10.5 mm configuration, and (d) the 12.5 mm configuration.

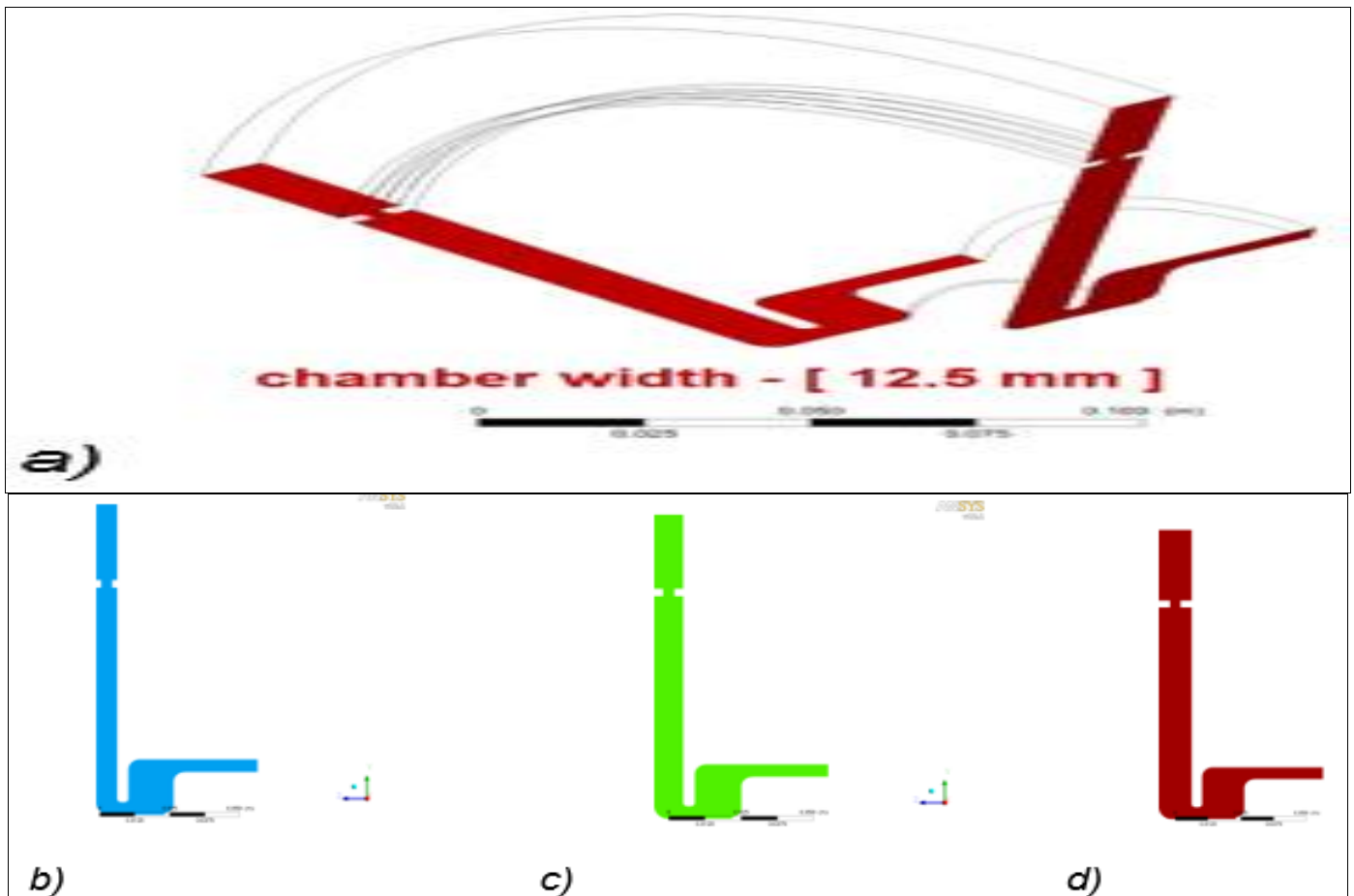


Fig 2.2: 90 Degree Segment

A simplified cavity model is a model for which vanes and blades are omitted and exclusively the front cavity of a turbine is considered. There is also a so called 1.5 stage full

cavity model, which is given in the Figure 2.3 and in which vanes as well blades are included.

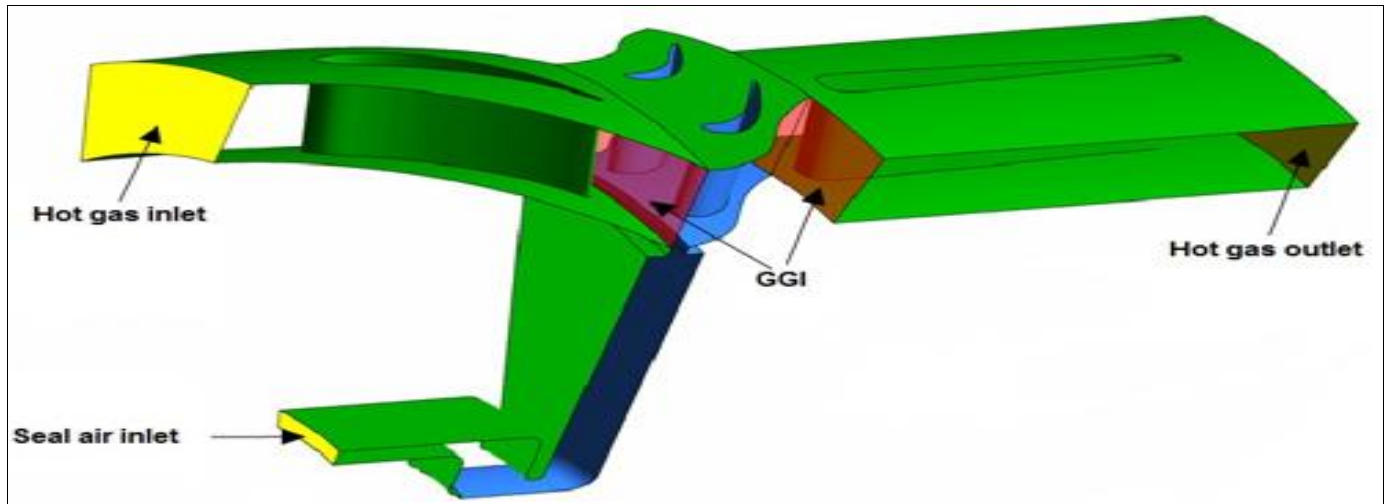


Fig 2.3: Full Cavity Model

The reason for preferring a simplified cavity is a less computational effort needed compared to the bigger full cavity model. As the vanes and blades are missing for the

simplified cavity model which is illustrated in the Figure 2.4, their influence has to be reflected on the hot gas inlet and outlet boundary conditions.

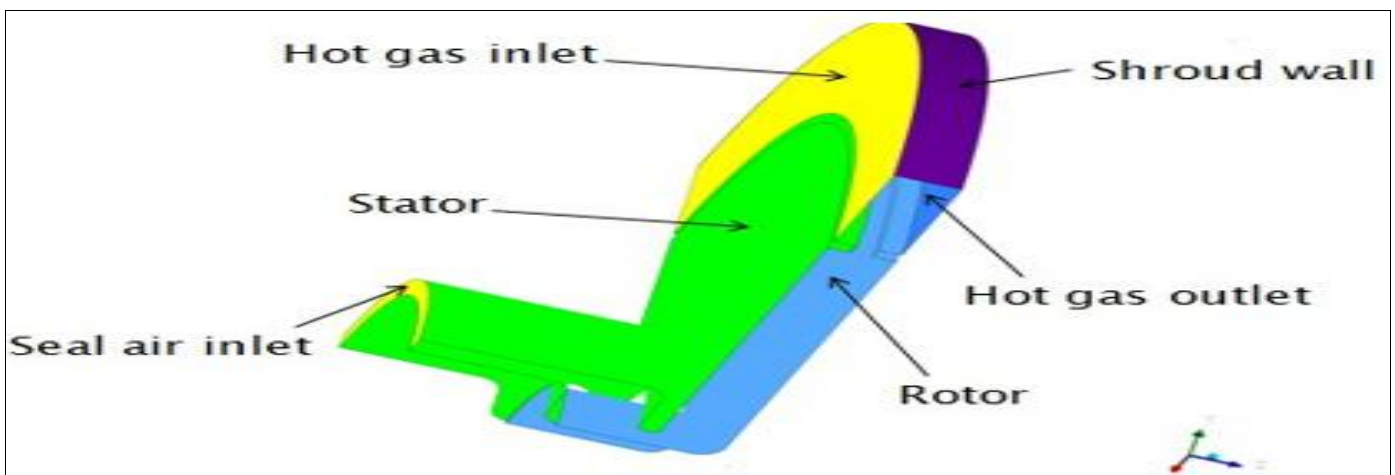


Fig 2.4: 90 Degree Segment Simplified Cavity Computational Model

Boundary conditions are of utmost importance in CFD analysis, as they directly affect the physical accuracy of the simulations. Two types were utilized in this work: averaged mean value and profile boundary conditions. Averaged mean value conditions are simpler and involve applying a spatial average of the velocity or pressure on a given boundary. These are computationally less expensive but tend to produce less accurate representations of real flow behavior. In contrast, profile boundary conditions use data extracted from full model simulations to define spatially varying values on the inlet and outlet surfaces. These profiles include detailed distributions of temperature, pressure, and velocity components and are essential for capturing complex flow phenomena like ingestion and vortex formation.

In the models used in this work, the outlet boundary condition was set to a constant pressure of 2.25 bar. For the

inlet, different velocity components were applied based on predefined flow angles. Radial velocity was neglected due to its negligible influence. Swirl-free assumptions, which involve setting the circumferential velocity component to zero, were not used as they have been shown to yield unrealistic flow fields in similar numerical studies.

The inlet velocity profiles were calculated using trigonometric relationships from the velocity magnitude and angle, as implemented via the Ansys-Postprocessor function calculator. This allowed the generation of accurate flow profiles that reflected experimental observations. The profile data include radial, tangential, and axial coordinates, as well as corresponding state variables. The standard profiles include 16 vanes and 32 blades, and their impact is indirectly captured through the imposed boundary conditions. Figure 2.5 illustrates the inlet velocity and outlet pressure profiles used in the simulations.

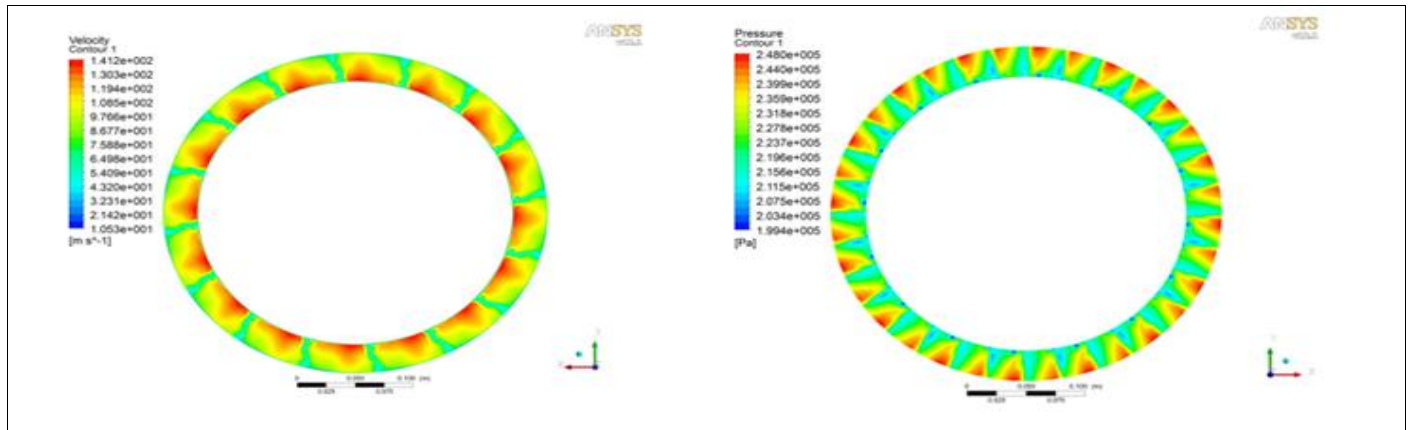


Fig 2.5: Inlet Velocity (Left) and Outlet Pressure (Right) Profiles

The meshing for all models was performed by M. Rabs using structured hexahedral grids, which are particularly suited for resolving the complex flow patterns expected in the cavity. A total of three mesh configurations were used,

each corresponding to one of the three cavity width sizes in the 22.5° segments. Their properties are given in the Table 2.1 below:

Table 1: Important Characteristic Values of the Segment Meshes

Mesh	Orthogonality Angle Minimum	Exponential Factor Maximum	Aspect Ratio
22.5deg. 12.5 mm cavity width	42.3	3	221
22.5deg. 10.5 mm cavity width	41.6	3	247
22.5deg. 7.5 mm cavity width	35.8	3	228

Furthermore, the total number of nodes for the meshes of the models used is given in the Table 2.2.

Table 2: Total number of nodes of the meshes in the models used

Models	Total number of nodes in model meshes
90 deg. segment standard	2,330,910
180 deg. segment standard	4,637,790
360 deg. full standard	9,227,520
90 deg. segment cavity width 7.5 mm	2,457,980
90 deg. segment cavity width 10.5 mm	2,483,394

To investigate the development of large-scale vortex structures, the simulations focused on low purge mass flow rates with a non-dimensional purge flow coefficient of 7000 as vortex formation was observed to occur only below certain threshold values according to experimental results from the test rig.

Both steady-state and transient simulations were carried out to evaluate the flow development. For all simulations, a Specific Blend Factor of 1 was used to ensure solution accuracy. In steady simulations, convergence was determined by evaluating outer loop residuals. In contrast, transient simulations relied on monitoring the inner loop

convergence within each time step. Each transient simulation was run with 10 to 12 inner loops per time step. Monitor points were defined to track variables such as sealing effectiveness and absolute pressure. These points were placed in key regions like the rim seal gap and the upper wheel-space cavity, where vortex activity is expected. The rotor speed for all simulations was 9000 revolutions per minute. Based on this speed, time steps corresponding to 0.3°, 0.5°, 1°, and 3° of rotor rotation were selected to study the sensitivity of the transient solution to time resolution. The selection of time steps allowed a balance between computational time and resolution accuracy.

III. RESULTS AND DISCUSSION

The Table 3 provides a summary of the simulations conducted.

Table 3: Overview of Simulation Variations

Boundary Condition	Variations
Surface-averaged hot gas boundary steady and transient	Flow Angle
Profile boundary conditions steady and transient	Number of Vanes and Blades for Profiles
	Amplitude of Pressure Outlet Profile
	Cavity Width

A. Surface Averaged Hot Gas Boundary Conditions

Both steady and transient simulations of the 90° segment model with averaged mean value boundary conditions were carried out and analyzed in this subchapter.

➤ *Steady Simulations*

To minimize computational cost and avoid the high computational demands of simulating a 360° full model, this study focused on the 90° segment model. The periodic flow

behavior was ensured using domain interfaces as periodic boundaries. A mean absolute inlet velocity of 215.8 m/s was used as a reference value.

Previous work by Ellermann [6] involved simulations at inlet flow angles of 18° and 20°. To expand upon this, the present study included additional flow angles of 14° and 22°. Table 4 presents the axial and circumferential velocity components for each tested angle.

Table 4: Axial and Circumferential Velocity Components at Different Angles

Angle [°]	Axial [m/s]	Circumferential [m/s]
14	52.21	209.39
18	66.69	205.24
20	73.81	202.79
22	83.84	200.09

To enhance simulation accuracy, high-resolution turbulence numerics were applied. Unlike Ellermann's model [6], which excluded the seal air flow path, the current model includes it. This led to a significant reduction in reverse flow at the outlet. For instance, at 20°, the portion of the outlet boundary recognized as wall by the Solver decreased from 36.1% to 26.9% for faces and from 7.6% to

3.4% for surface area. This reduction helped prevent simulation failures that had occurred in earlier studies.

The simulation result at 18° served as the basis for further computations. Figure 5.1 shows the pressure contours plotted on an axial plane located 0.05625 mm downstream of the stationary disc, with a radius of 0.135 m.

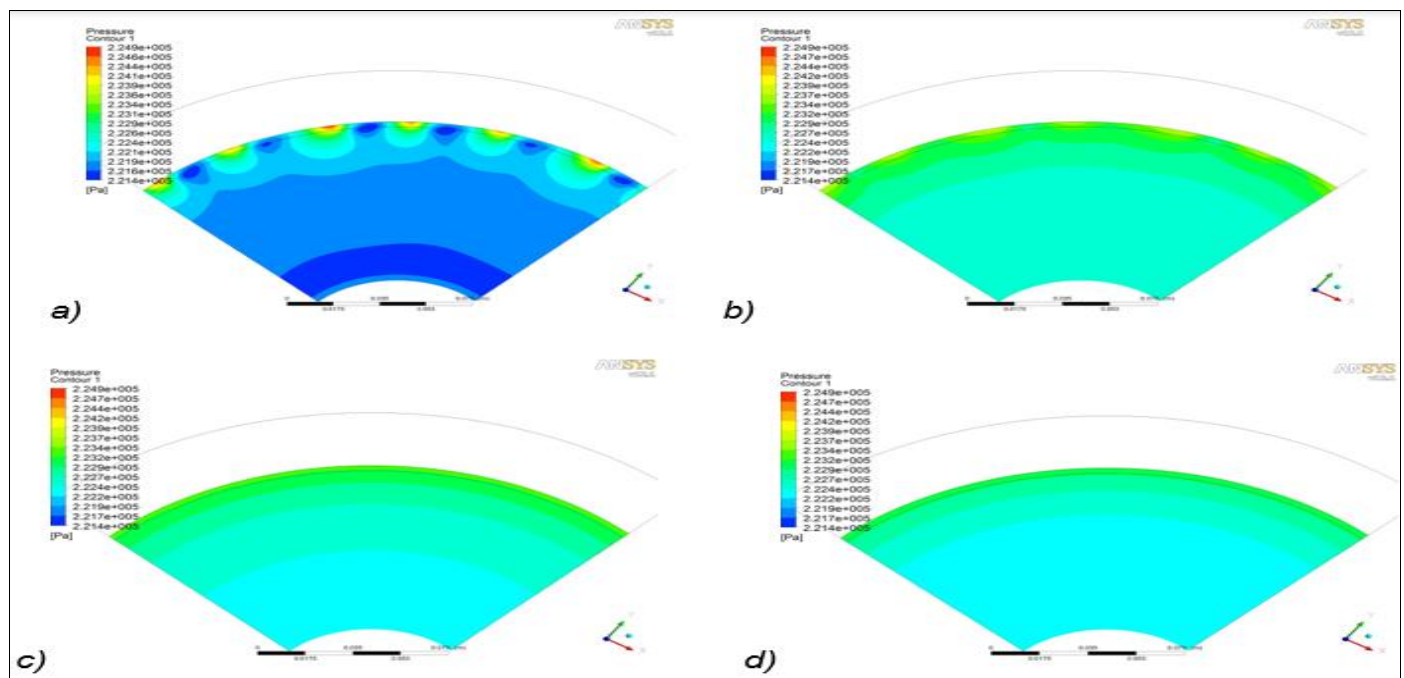


Fig 3.1: The Pressure Contour Plots for Steady Simulation with Hot Gas Averaged Boundary Conditions
a) 14° b) 18° c) 20° d) 22°

No large-scale rotating vortex structures were observed for any of the tested angles, as anticipated. This corresponds with earlier findings that constant boundary conditions in 90° models do not support vortex development. Ellermann's simulations had shown Kelvin-Helmholtz instabilities at 18° and 20°, but these were not reproduced in the current steady simulations. Minor fluctuations were seen in the 14° case, but they did not evolve into coherent vortex structures. The 18° simulation exhibited weak instabilities, while both 20° and 22° showed relatively smooth and stable flow behavior, with 22° being the most uniform. Differences from earlier

studies are likely due to differences in both model geometry and the boundary conditions applied. This study used a turbulence intensity of 5% at the inlet, compared to the k-ε turbulence model used by Ellermann [6].

As the inlet angle increases, the circumferential velocity component decreases while the axial component rises. This shift supports flow stabilization, as the circumferential velocity tends to promote instability. Consequently, higher inlet angles contribute to more stable flow conditions.

Due to the inherent limitations of steady simulations in capturing time-dependent behaviors, transient simulations were carried out as detailed in the next subchapter.

➤ *Transient Simulations*

Because steady simulations did not yield notable vortex formations, transient simulations were performed using the 90° segment model with an 18° inlet flow angle. The results of the corresponding steady simulation were used as initial conditions.

The transient simulation was divided into two stages. The first stage ran over 8.2 revolutions with a time step corresponding to 3° rotation, allowing for extended physical time coverage though with reduced precision. The second stage added 3.2 revolutions using a finer time step of 1° rotation to improve accuracy.

Although the steady results had shown minor flow irregularities, the transient simulation magnified these into noticeable instabilities in the rim-seal cavity. These were attributed to the superposed shear layer formed by the interaction between the cavity flow and the incoming hot gas through the rim seal.

Figure 3.2 presents the final pressure contour and velocity vector plots. The velocity vectors are shown in the vortex reference frame, which highlights the rotational characteristics of the flow. Since Ansys does not provide a built-in option for vector transformation into this frame, a user-defined session file was used to perform the transformation based on derived expressions. This transformation allowed for a clearer representation of the dynamic flow behavior.

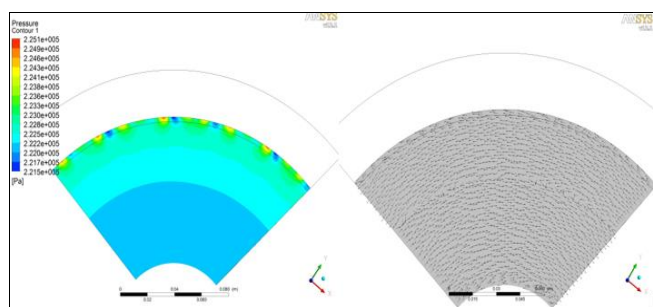


Fig 3.2: The pressure contour and velocity plots for transient simulation with hot gas averaged boundary condition

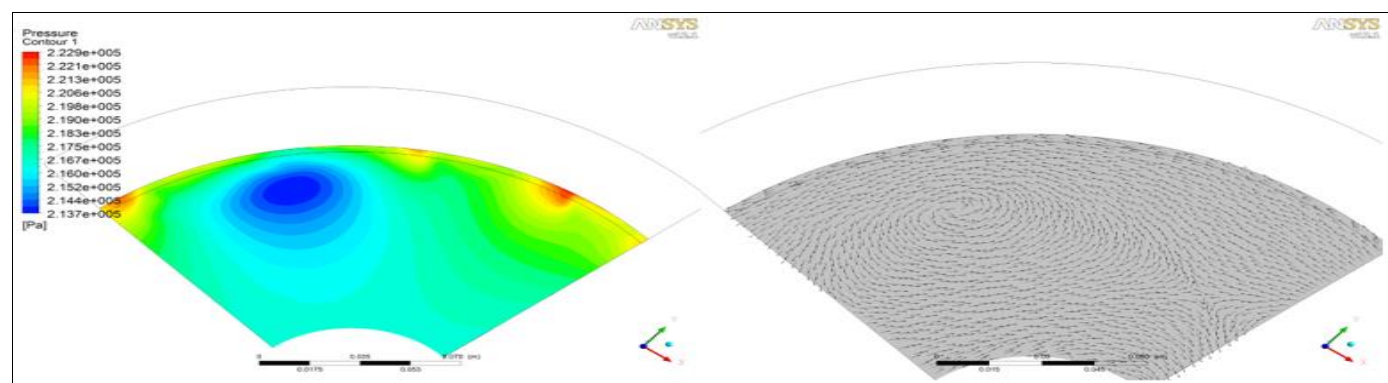


Fig 3.3: Pressure Contour (Left) and Vector Velocity Field(Right) Plots

Despite the intensified fluctuations, no coherent large-scale vortex formations appeared in the wheel-space cavity, as evident from Figure 5.2. This supports the understanding that averaged hot gas boundary conditions do not sufficiently replicate the flow conditions needed to initiate such structures.

These results underscore the critical role of boundary condition realism in CFD modeling. As will be elaborated in subsequent chapters, the use of profile-based boundary conditions allows for a more accurate reproduction of flow instabilities and vortex structures in the cavity region.

B. Surface Averaged Hot Gas Boundary Conditions

➤ *Standard Profiles*

This section examines the computational results obtained using standard flow profiles on three geometrical configurations: the 90°, 180°, and 360° segment models. Each model’s steady and transient simulations were critically evaluated to assess their ability to reproduce large-scale rotating structures in the wheel-space cavity.

The 90° segment model, generated by multiplying a 22.5° periodic sector four times, is widely used due to its reduced computational demand. Despite past investigations showing limited realism, further simulations were performed to investigate underlying numerical issues and to explore the model’s potential.

In the steady simulation, a previously computed result using averaged mean boundary conditions at an 18° flow angle served as the initial condition. After 400 iterations, a clear large-scale rotating structure developed, implying four such structures in the full 360° model. This observation corresponds to earlier findings by Ellermann [6].

The resulting pressure contour and vector velocity field are shown in Figure 3.3. Further analysis of the vortex formation process was conducted using streamline

visualizations in both the stationary, and vortex reference frames. These are depicted in Figure 3.4.

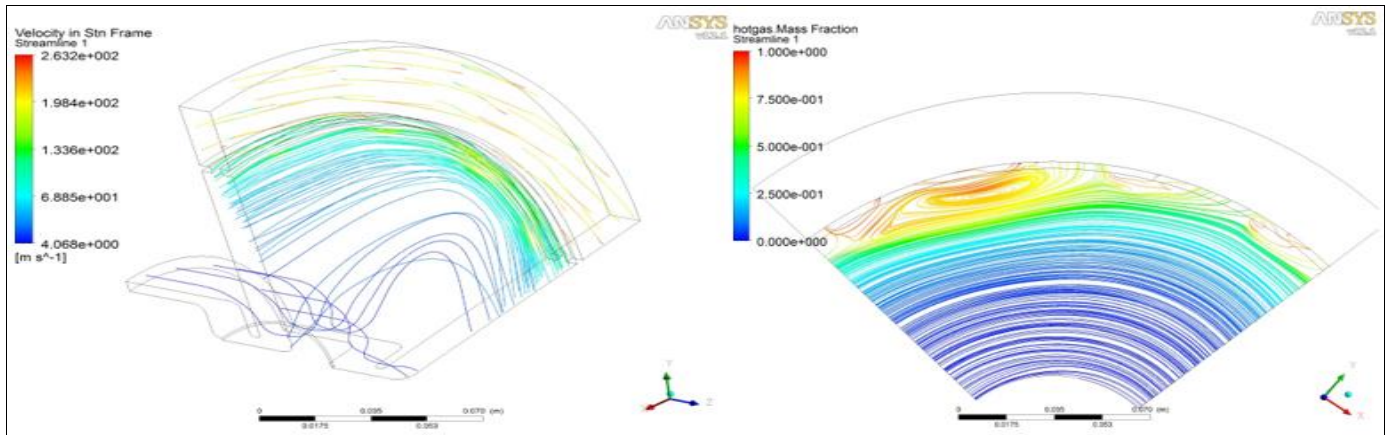


Fig 3.4: a) 3D velocity streamlines in the stationary reference frame b) Hot gas ingestion streamlines in the vortex reference frame

The streamline plots reveal that hot gas ingestion occurs predominantly in the region where the vortex structure develops. The tangential velocity of the hot gas flow is higher than that of the inner cavity flow, creating a strong shear layer that promotes the formation of a rotating structure.

To capture the time-evolving behavior of these structures, transient simulations were initiated. The initial time step used was equivalent to a 3° rotor rotation. Although computationally efficient, this time step resulted in an early disappearance of the vortex structure seen in the steady simulation. To understand this phenomenon, velocity vector fields and pressure contours were evaluated every half a revolution over 1.5 revolutions. The vortex structure diminished steadily, becoming weaker and less distinct. Initially present low-pressure zones associated with vortices became harder to identify. Another small, weaker vortex briefly entered the domain but failed to grow. This decline in structure strength may be due to numerical dissipation, model size, and limitations posed by the periodic

boundaries. The vortex took approximately 2.5–3 rotor turns to completely vanish. A noticeable deceleration of the vortex near the domain interface was recorded, with its speed estimated to be between 60–70% of the rotor speed using isosurface tools.

The simulation was continued with the 3° time step for an additional 680 iterations, equating to approximately 5.67 revolutions. Though the pressure and sealing effectiveness at monitoring points displayed periodicity, the pressure amplitude was too small to trigger vortex reformation. To improve resolution, the time step was reduced to 1° and later 0.5°, simulating another full revolution. However, these smaller steps also failed to regenerate distinct vortex structures.

To assess local pressure behavior, absolute pressure values at monitor point 16 (located at 0.12 m radius in the upper wheel-space cavity) were tracked. These are shown in Figure 5.7.

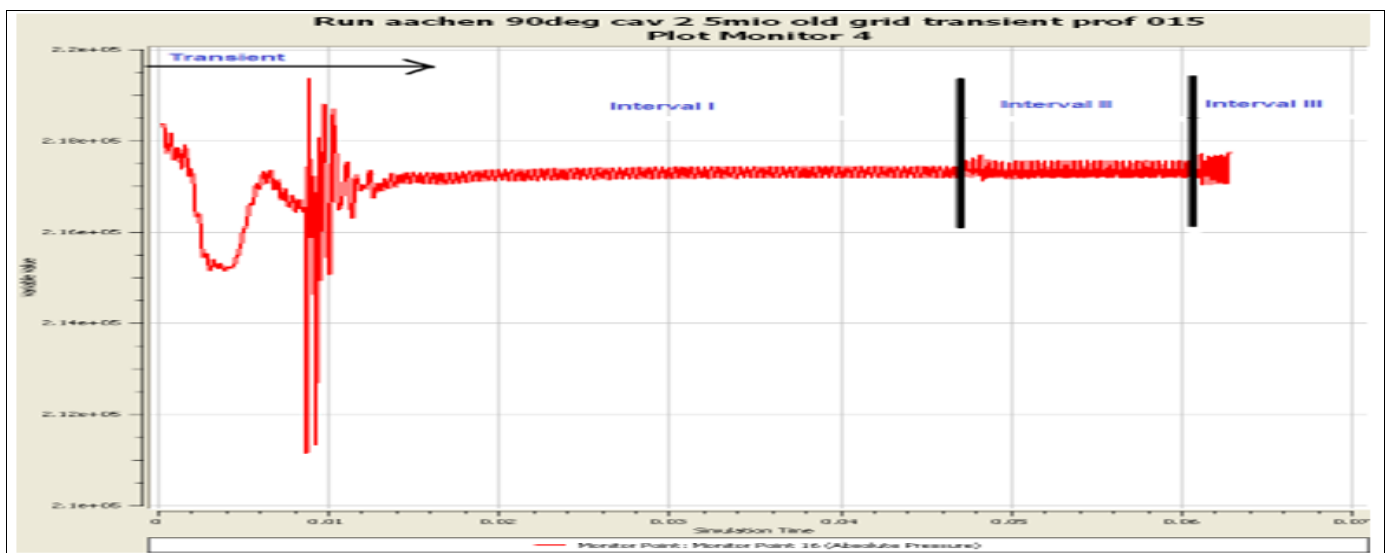


Fig 3.5: Absolute Pressure Run on Monitor Point 16

Figure 3.5 shows increased amplitude with decreasing time step, indicating higher resolution. The initial simulation stage experienced strong perturbations, likely caused by the transition from steady to unsteady conditions. A stable periodic pattern was reached after approximately 300–350 time steps, aligning with the observed disappearance of the vortex.

The analysis indicates that despite finer time steps, the 90° model fails to regenerate large-scale rotating structures under standard profiles. The results suggest that the periodic boundary conditions used in this model may suppress vortex development. Although it might be argued that such structures could disappear in real flow after some revolutions, experimental studies from the Technical University of Aachen have shown persistent vortex presence, challenging this assumption.

To reduce the limiting effects of periodic boundaries, simulations were performed on the 180° segment model. The increased domain size enhances the likelihood of capturing realistic flow phenomena.

In the steady simulation, one complete and two partial vortex structures were identified, forming a triangular

configuration. This infers the presence of four large-scale rotating structures in a full 360° annulus.

The unsteady nature of vortex dynamics prompted the continuation of transient simulations. Using results from the steady run as the initial condition, the simulation was advanced with a 3° time step. Similar to the 90° model, all vortices disappeared after the first full revolution. The simulation continued for a total of 2.3 revolutions. Once initial transients were resolved, vortex structures no longer appeared. To improve accuracy, a finer time step of 1° per rotor angle was applied for one complete revolution. As with previous results, no vortex structures re-emerged. The simulation shows minor instabilities in the rim seal cavities, but none develop into distinct vortex structures. Again, the persistence of periodic boundaries is suspected to limit the formation of such structures.

The 360° full model, which avoids periodic boundaries, offers the most realistic simulation environment. Both steady and transient simulations were carried out. In the steady simulation, conducted over 2000 iterations, one pronounced vortex and two weaker low-pressure zones were identified. These are depicted in Figure 3.6.

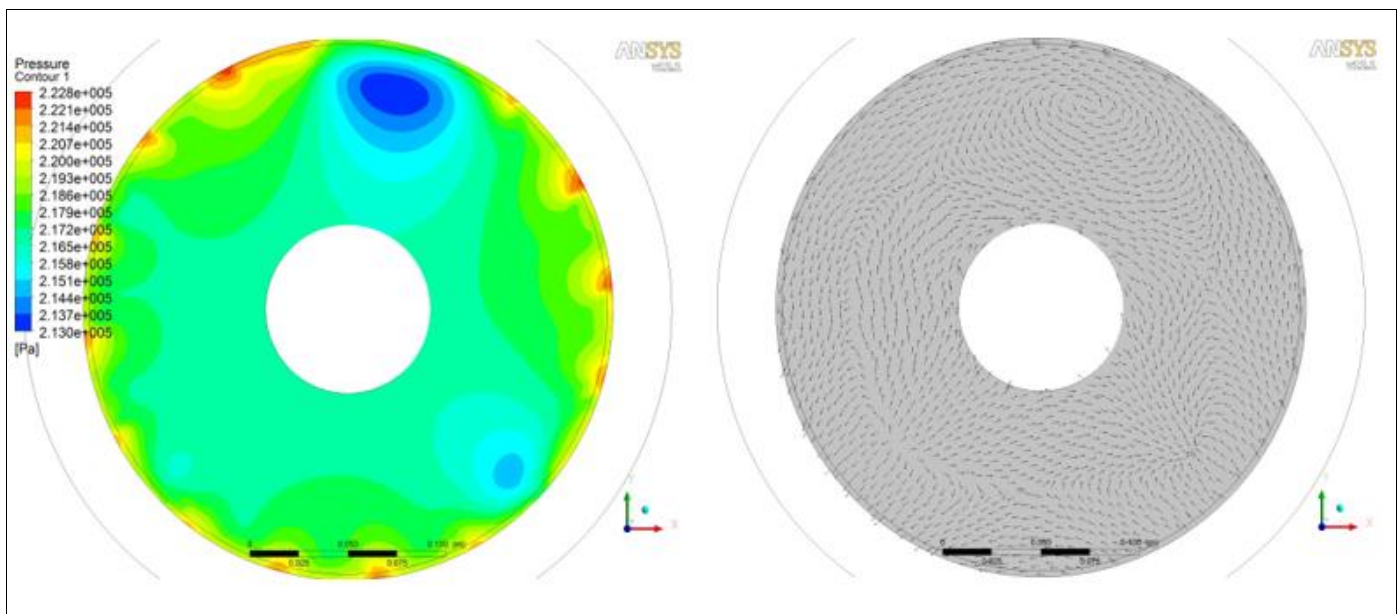


Fig 3.6: Pressure Contour and Vector Velocity Field Plot for Steady Simulation with 360° Model

Previous studies by Jakoby [3] on the ALSTOM test rig identified three vortex structures in a Mercedes-star pattern, shown for comparison in Figure 3.7.

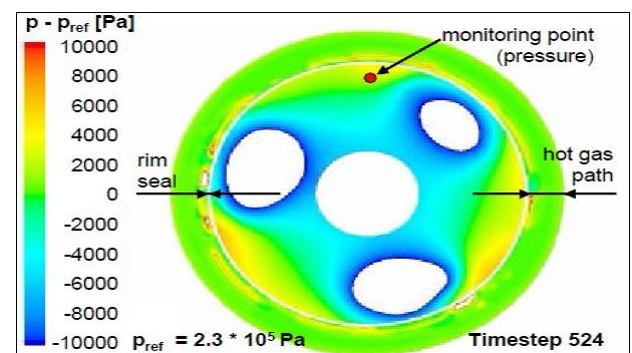


Fig 3.7: ALSTOM Unsteady Simulation Results with Hot Gas Averaged Boundary Conditions [3]

A similar tendency was observed in the present study. The steady simulation revealed early development toward a comparable vortex pattern, though two of the structures remained underdeveloped.

A transient simulation was initiated using a fine time step of 0.3° per rotor angle to track the decay process. The vortex structure's intensity and size decreased progressively. The early phase simulation was stopped at 150° due to high computational cost. Subsequently, the time step was increased to 1° for another 120° , followed by a return to 0.3° to observe early dissipation. Despite these efforts, vortex structures vanished entirely within 1.3 revolutions—sooner than the 2.5–3 revolutions observed for smaller segment models. An additional revolution with a 1° time step did not restore vortex structures. This outcome supports similar findings from Ellermann [6], where vortex disappearance persisted even after six revolutions.

Together, these results confirm that while the 360° model offers a better framework for capturing realistic flow dynamics, vortex persistence remains elusive under standard profile conditions. More targeted variations in boundary profiles are needed to promote sustained vortex structures, as explored in the next section.

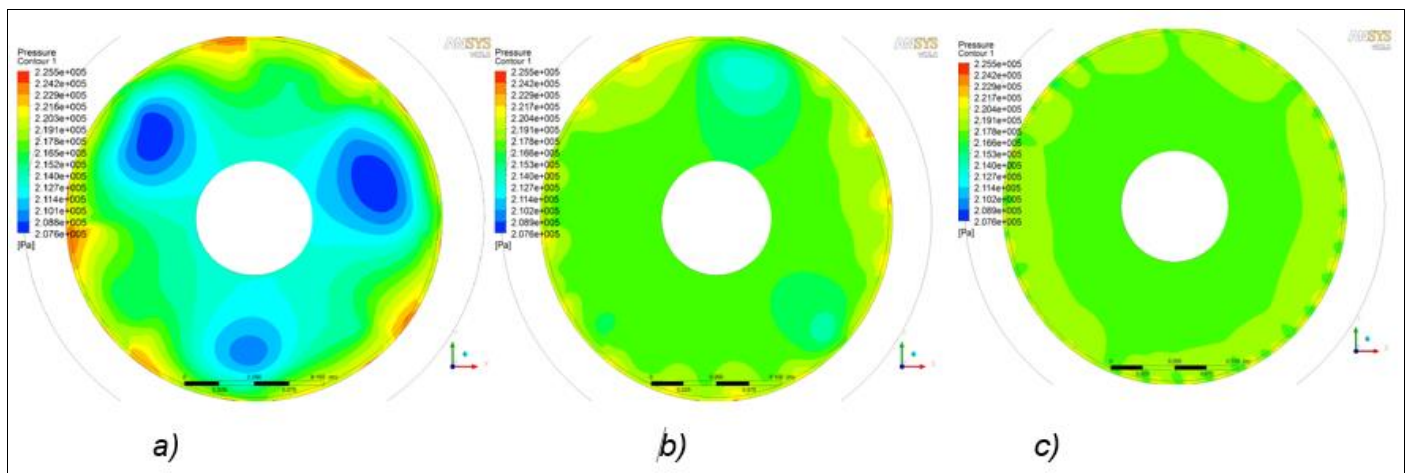


Fig 3.8: Pressure Contour Plots for Steady Simulations: a) 8–16 b) 16–32 c) 32–64 Vane-Blade Profiles

Transient simulations further emphasized the differences. Each configuration was run over four rotor revolutions using time steps of 3° and 1° . The 8–16 profile displayed unsteady flow and up to four vortex structures forming and dissipating during the run. The 16–32 and 32–64 configurations however remained mostly laminar and showed no vortex formation.

These results indicate that while pressure amplitude affects the intensity of hot gas ingestion and flow unsteadiness, it does not by itself initiate vortex formation unless combined with an appropriate blade/vane configuration. The number of vanes and blades has a greater influence on the circumferential pressure distribution, which is critical for generating the shear interfaces necessary for vortex development.

➤ Variations in the Profiles

This section explores how variations in the boundary profile conditions affect the development of vortex structures within the wheel-space cavity. Two primary types of profile modifications were considered: changes in the number of vanes and blades, and alterations in the pressure amplitude in the outlet profiles. The impact of these variations was evaluated through both steady and transient CFD simulations.

The standard configuration, based on the test rig at the Technical University of Aachen, uses 16 vanes and 32 blades. To assess the sensitivity of vortex formation to blade/vane count, two additional profiles were created: one with fewer components (8 vanes, 16 blades) and one with more (32 vanes, 64 blades).

The steady-state simulation for the 8–16 setup led to the formation of three distinct large-scale rotating structures, while the 16–32 case showed one. The 32–64 profile produced no visible vortex structures. These results are visualized in Figure 3.8.

In conclusion, the formation of large-scale rotating structures is most effectively influenced by reducing the number of vanes and blades in the boundary profiles. Increasing the outlet pressure amplitude introduces unsteady flow behavior but does not alone produce coherent vortices. These insights can inform the design of future simulation setups and boundary condition strategies.

➤ Variations in Cavity Width

The cavity width is the distance between rotor and stator surfaces in the wheel-space. The standard model features a 12.5 mm cavity width. For comparison, variants with 7.5 mm and 10.5 mm widths were analyzed using 90° segment models. Both steady and transient simulations were conducted to assess the influence of geometry on flow behavior.

Initial steady-state simulations were executed for each width variant, running for 2000 iterations. Pressure contours

and velocity vector plots were evaluated, as presented in Figure 5.22.

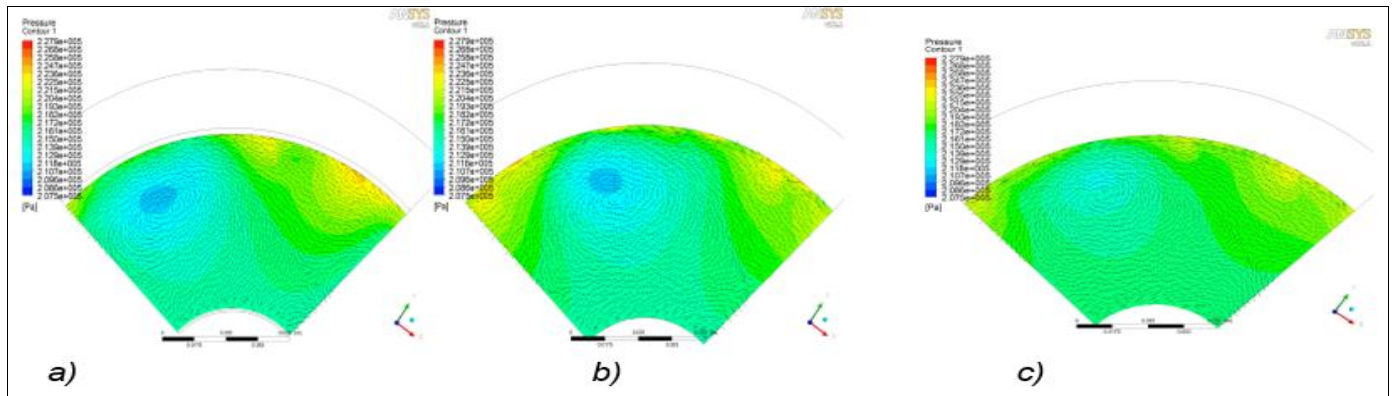


Fig 3.9: Pressure Contour and Velocity Vector Plots with Cavity Widths a) 7.5 mm b) 10.5 mm c) 12.5 mm

The vortex structures developed in all cavity width variations. However, the vortex structure became less distinct in the pressure contour plot with the increasing cavity width sizes. In the given range in the pressure contour, the model with 7.5 [mm] has the most distinct, while the model with 12.5 [mm] has the least distinct large scale rotating structure. This is also reflected in the absolute pressure run, where the amplitude increases with the decreasing cavity width size.

Subsequent transient simulations used a time step of 5.55556×10^{-5} s per 3° , running approximately 7.5 revolutions. The 7.5 mm model maintained a strong vortex throughout the simulation, whereas the 10.5 mm model's vortex dissipated after roughly 2–2.5 turns. These results indicate that narrower cavity widths promote persistent vortex activity, while mid-sized cavities may dampen unsteady flow structures.

In conclusion, a reduced cavity width of 7.5 mm enhances vortex strength and longevity. The 10.5 and 12.5 mm variants fail to sustain vortex structures despite early development. These outcomes reinforce the role of cavity geometry in rim cavity flow behavior under CFD analysis.

IV. CONCLUSION

The objective of this work is to numerically demonstrate the existence of vortex structures within the front cavities of gas turbines. This investigation builds upon previous studies conducted at the university, where hot gas boundary conditions were used. However, those earlier simulations failed to produce realistic results. Consequently, this study shifts focus to profile boundary conditions, aiming to better replicate the development of vortex structures in rim cavities.

Before implementing profile boundary conditions, baseline simulations were carried out using hot gas averaged boundary conditions. These simulations, performed on a 90° segment model, did not reveal any formation of vortex structures. This finding highlights the potential role of circumferential hot gas flow as a critical factor in vortex development.

Following this, a series of simulations incorporating profile boundary conditions were undertaken using three different computational domains: 90° , 180° , and 360° models. The boundary conditions were derived from data collected through measurements at the Technical University of Aachen. All three models successfully produced vortex structures during steady-state simulations. However, during transient simulations, vortex structures gradually dissipated after 2–3 rotor revolutions. Given the inherently unsteady nature of flow in rim cavities, the inability of transient simulations to sustain vortex structures necessitated a deeper investigation using modified profile conditions.

To eliminate the influence of periodic boundary conditions—which are known to suppress vortex formation—all further analyses were limited to the 360° full model. This allowed for a clearer evaluation of the effects of varying profile boundary conditions. The first set of variations focused on altering the number of vanes and blades in the profiles. Reducing the number of vanes and blades led to the formation of distinct vortex structures in both steady and transient simulations. Conversely, increasing their number resulted in the complete absence of vortex structures. This outcome is attributed to the changes in circumferential pressure distribution caused by differing vane-blade counts along the outlet boundary surface.

The second variation involved modifying the amplitude of the outlet pressure profiles while maintaining the 360° model. Pressure amplitudes were increased for outlet profiles with both reduced and increased vane-blade counts. In the case of reduced vane-blade profiles, the increased amplitude generated a higher level of flow instability. Despite this, the number of developed vortex structures was not enhanced; instead, it decreased for both steady and transient runs. An additional observation revealed that vortex structures in this case tended to form deeper within the cavity—closer to the central region—which can be explained by elevated pressure levels in the hot gas annulus. Meanwhile, profiles with increased vane-blade counts did not show any significant change in behavior due to amplitude adjustments.

Further analysis involved altering the cavity geometry. Specifically, the cavity width was varied from the standard 12.5 mm to narrower widths of 10.5 mm and 7.5 mm. The results revealed that decreasing the cavity width contributed to the emergence of vortex structures in both steady and transient scenarios. This effect is most likely due to the increased instability introduced by the reduced axial gap between rotor and stator walls.

Based on these findings, it is clear that continued investigation into vortex structures in wheel-space cavities is warranted. One of the key limitations in this study has been the computational and temporal demands of transient simulations, particularly those involving the 360° full model. Future work must address these constraints by allocating greater computational resources and utilizing finer time steps to better capture transient flow behavior. The use of full annular models, as opposed to periodic segments, is crucial for achieving accurate, reality-close predictions of vortex phenomena.

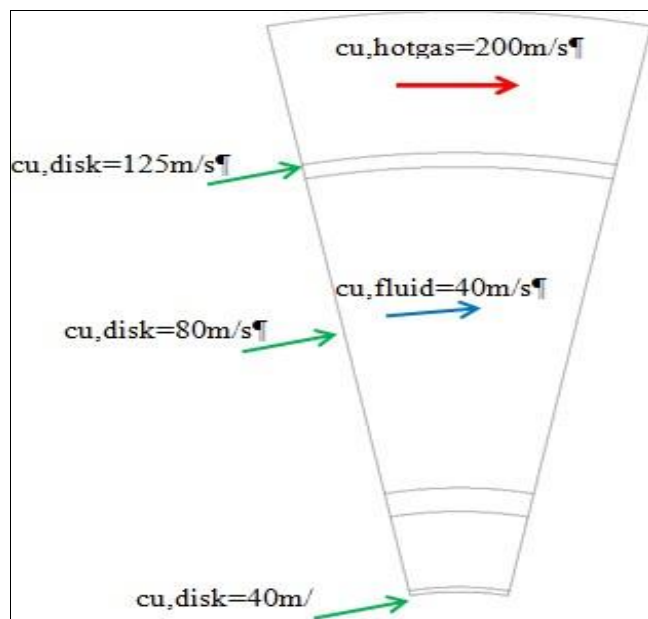


Fig 4.1: Vortex Structure Development

As illustrated in Figure 4.1, the development of vortex structures is driven by a velocity differential between the hot gas and cavity flow. The hot gas, with a tangential velocity component of approximately 200 m/s, enters the cavity and interacts with the inner cavity flow. Because the tangential speed of the ingested hot gas exceeds both the disk rotation

speed and the tangential velocity of the cavity flow (which is scaled by a factor $\beta < 1$), a shear layer is formed. In the rotor reference frame, the hot gas flow is positive, while the cavity flow is negative. This velocity shear initiates a roll-up mechanism that eventually develops into large-scale rotating structures.

Future research should prioritize experimental validation to further understand the flow behavior in these cavities. In particular, the vertical structure and origin of flow perturbations should be examined. A more detailed understanding of the impact of cavity and seal geometry on vortex formation will significantly enhance predictive modeling capabilities in gas turbine design.

REFERENCES

- [1]. Rolls-Royce: The Jet Engine, ISBN 0-902121-04-9
- [2]. Cao, C., Chew, J.W., Millington: "Interaction of Rim Seal and Annulus Flow in an Axial Flow Turbine J. of Eng. for Gas Turbines and Power", 126(4), October, pp.786-793.
- [3]. Jakoby, R., Zierer, T., Lindblad, K., Larsson, J., deVito, L., Bohn, D.E., Funcke, J., and Decker: "Numerical Simulation of the Unsteady Flow Field in an Axial Gas Turbine Rim Seal Configuration" ASME Paper GT2004-53829.
- [4]. Steve Julien, Julie Lefrancois, Guy Dumas, Guillaume Boutet-Blais, Simon Lapointe: "Simulations of flow ingestion and related structures in a turbine disc cavity"
- [5]. M.Rabs, F.-K. Benra, H. J. Dohmen . "Investigation of the flow instabilities near the rim cavity of a 1.5 stage gas turbines" ASME Paper GT2009-59965
- [6]. Lars Ellermann: Studienarbeit, "Numerische Untersuchung der rotierenden Niederdruckfeldern in Radseitenräumen von Gasturbinen"
- [7]. Hills, N.J., Chew, J.W. and Turner: "Computational and mathematical modelling of turbine rim seal ingestion", ASME Turbo Expo paper 2001-GT-204 (Also ASME J. Turbomachinery, 2002, vol. 124, pp 306-315).
- [8]. Chen, J-X: Alstom internal report, Whetstone, U.K.
- [9]. King, M., Wilson, M. and Owen, M., 2005, "Rayleigh-Bénard Convection in Open and Closed Rotating Cavities" ASME Turbo Expo 2005, paper No. GT 2005-68948
- [10]. David Apsley: Lecture scripts "Introduction to CFD"